Circular Dichroism and Magnetic Circular Dichroism Spectroscopic Studies of the Non-Heme Ferrous Active Site in Clavaminate Synthase and Its Interaction with α-Ketoglutarate Cosubstrate

Elizabeth G. Pavel,[†] Jing Zhou,[†] Robert W. Busby,[‡] Michele Gunsior,[‡] Craig A. Townsend,*[,‡] and Edward I. Solomon*[,†]

Contribution from the Department of Chemistry, Stanford University, Stanford, California 94305, and the Department of Chemistry, The Johns Hopkins University, Baltimore, Maryland 21218

Received July 17, 1997

Abstract: Clavaminate synthase (CS) is one member of a large class of non-heme iron enzymes that require α-ketoglutarate (α-KG) as a cosubstrate. While the majority of this class catalyzes the hydroxylation of unactivated C−H bonds, CS is unusual in that in addition to performing hydroxylation chemistry, it also catalyzes the key oxidative ring closure and desaturation steps in the biosynthetic pathway to the potent *β*-lactamase inhibitor clavulanic acid. A single non-heme Fe^{2+} site is responsible for all three of these reactions (hydroxylation, oxidative ring closure, and desaturation), during which 1 equiv of α-KG per reaction is decarboxylated into succinate and CO_2. We have applied circular dichroism (CD), magnetic circular dichroism (MCD), and variable-temperature, variable-field (VTVH) MCD spectroscopies to probe the geometric and electronic structure of the ferrous active site in the isozyme CS2 and its interaction with α-KG. CD titration experiments show stoichiometric binding of Fe^{2+} to the apoenzyme, either with or without α-KG, as well as stoichiometric binding of α-KG to the iron-containing enzyme. However, in the absence of the metal, the α-KG binding constant is reduced, indicating that Fe^{2+} facilitates cosubstrate binding at the active site. Ligand field CD and MCD data show that resting CS2 contains a six-coordinate ferrous center ($10Dq = 10\ 050\ cm^{-1}$, $\Delta^5E_g = 1690\ cm^{-1}$) and that addition of α-KG perturbs the site to produce a different six-coordinate center ($10Dq = 9500\ cm^{-1}$, $\Delta^5E_g = 1630\ cm^{-1}$). VTVH MCD analysis finds a ground-state splitting for resting CS2 ($\Delta^5T_{2g} \approx -400\ cm^{-1}$) that is fairly typical of six-coordinate ferrous sites, but a much larger splitting for CS2 + α-KG ($\Delta^5T_{2g} \approx -1000\ cm^{-1}$), indicative of Fe^{2+}−α-KG *π* interactions. UV/vis absorption, CD, and MCD spectroscopies have been applied to further probe the interaction of the cosubstrate with the metalloenzyme. These data show the appearance of low-lying metal-to-ligand charge-transfer transitions which demonstrate that α-KG binds directly to the iron. Furthermore, analysis and comparison to model complex data support a bidentate binding mode of α-KG, indicating that cosubstrate displaces two ligands from the six-coordinate resting active site to form a new six-coordinate α-KG-bound Fe^{2+} site. These results provide the first direct spectroscopic information about the nature of the CS2 ferrous active site and its interaction with α-KG and lend insight into the mechanism of this multifunctional enzyme.

Introduction

Mononuclear non-heme iron enzymes catalyze a variety of important reactions involving the binding and activation of dioxygen.[1,2] One large class of non-heme enzymes is the α-ketoglutarate (α-KG)-dependent dioxygenases, which require Fe^{2+}, α-KG, and O_2 for catalysis and are found in animals, plants, and microorganisms.[3−5] Some of these include prolyl 4-hydroxylase and lysyl hydroxylase, which are involved in collagen biosynthesis;[6] thymine hydroxylase, which catalyzes three successive oxidations of thymine;[7] 4-hydroxyphenylpyruvate, which participates in the catabolism of tyrosine and whose substrate contains an internal α-keto acid;[8] and deacetylcephalosporin C synthase (DACS) and deacetoxycephalosporin C synthase (DAOCS), which are involved in the synthesis of cephalosporin and cephamycin antibiotics.[9,10] The α-KG-dependent enzymes are thought to share a common mechanism involving hydroxylation at unactivated carbon centers with the concomitant two-electron oxidation of the α-KG cosubstrate to succinate and CO_2, during which one atom of O_2 is incorporated into the hydroxylated product and the other appears in succinate (Scheme 1).

Clavaminate synthase (CS) is similar to other α-KG-dependent enzymes in that it catalyzes the hydroxylation of deoxyguanidinoproclavaminic acid to guanidinoproclavaminic acid,[11]

[†] Department of Chemistry, Stanford University.
[‡] Department of Chemistry, The Johns Hopkins University.

(1) Feig, A. L.; Lippard, S. J. *Chem. Rev. (Washington, D.C.)* **1994**, *94*, 759−805.
(2) Que, L., Jr.; Ho, R. Y. N. *Chem. Rev. (Washington, D.C.)* **1996**, *96*, 2607−2624.
(3) Prescott, A. G. *J. Exp. Bot.* **1993**, *44*, 849−861.
(4) De Carolis, E.; De Luca, V. *Phytochemistry* **1994**, *36*, 1093−1107.
(5) Hedden, P. *Biochem. Soc. Trans.* **1992**, *20*, 373−377.
(6) Kivirikko, K. I.; Myllylä, R. In *The Enzymology of Post-translational Modification of Proteins*; Freedman, R. B., Hawkins, H. C., Eds.; Academic Press: London, 1980; Vol. 1, pp 53−104.
(7) Thornburg, L. D.; Lai, M.-T.; Wishnok, J. S.; Stubbe, J. *Biochemistry* **1993**, *32*, 14023−14033.
(8) Lindstedt, S.; Odelhög, B.; Rundgren, M. *Biochemistry* **1977**, *16*, 3369−3377.
(9) Jensen, S. E.; Westlake, D. W. S.; Wolfe, S. *J. Antibiot.* **1985**, *38*, 263−265.
(10) Baldwin, J. E.; Abraham, E. *Nat. Prod. Rep.* **1988**, *5*, 129−145.

S0002-7863(97)02408-6 CCC: $15.00
Published on Web 01/16/1998

Scheme 1

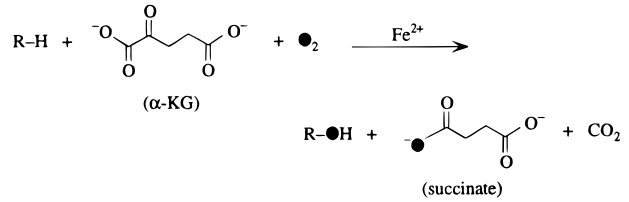

as shown in the first step of Scheme 2. Additionally, CS catalyzes the oxidative ring closure of proclavaminic acid to dihydroclavaminic acid and subsequent desaturation to clavaminic acid (second and third steps in Scheme 2) in a four-electron process requiring 2 equiv of both α-KG and O_2.[12] Although one atom of dioxygen is incorporated into α-KG and released as succinate, the other oxygen atom is not incorporated into product, but is instead reduced to H_2O in the cyclization/desaturation reactions.[13] This marks a strong deviation of CS from other α-KG-dependent enzymes and is similar to isopenicillin *N* synthase (IPNS), which catalyzes oxidative ring closure through a sulfur heteroatom, but does not require α-KG.[14]

CS is of particular interest because of its ability to execute the key ring closure step in the biosynthesis of clavaminic acid, the precursor of clavulanic acid which is a potent β-lactamase inhibitor. The enzyme has been isolated from clavulanic acid-producing *Streptomyces clavuligerus* as two isozymes, CS1 (M_r 35 347) and CS2 (M_r 35 774), whose kinetic and physical properties are very similar.[15] The corresponding genes have been cloned and sequenced, and comparison shows 82% identity and 87% similarity between *cs1* and *cs2*, with significant homology in the central region, but extremely little homology with other α-KG-dependent enzymes or IPNS.[16] The genes have been overexpressed in *E. coli* to yield soluble protein whose properties are in excellent agreement with those of the wild-type enzymes.[17,18] Our studies will focus on CS2, which is the isozyme that resides in the gene cluster responsible for clavulanic acid biosynthesis.[19]

Proposed mechanisms for CS invoke sequential kinetics and begin with the binding of Fe^{2+}, α-KG, O_2, and substrate. This is followed by oxidative decarboxylation of α-KG to yield succinate, CO_2, and a reactive iron−oxygen species,[15,20] proposed to be a ferryl ion for other α-KG-dependent enzymes.[21−23] In the hydroxylation reaction, this reactive iron species inserts oxygen to hydroxylate deoxyguanidinoproclavaminate substrate

Scheme 2

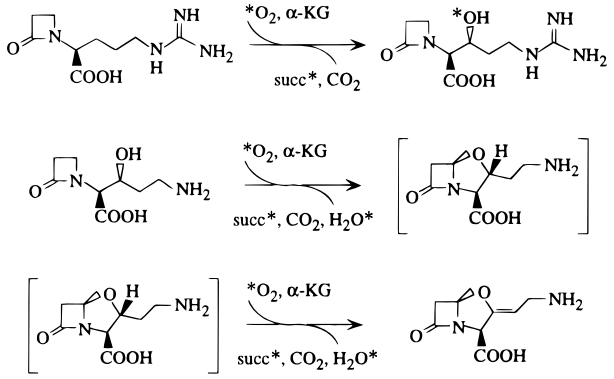

with retention of configuration.[24] In the cyclization/desaturation reactions, proclavaminate substrate may bind through the C-3 hydroxyl group to the reactive iron species, which has become more electrophilic.[25] This hypothesis is supported by a recent crystal structure of IPNS which shows the substrate bound directly to the iron through the S atom at which cyclization occurs.[26] Through analogy with P-450 mechanisms, homolytic C−H abstraction by the reactive iron−oxygen species is proposed to form a carbon-centered radical (or possible organo-iron species),[20] resulting in the cyclization of substrate to produce dihydroclavaminate and the release of water. Thus instead of conventional dioxygenase activity, CS promotes radical (or cation) capture *intra*molecularly with substrate-derived oxygen rather than *inter*molecularly with a O_2-derived species.[20] Consistent with a stepwise mechanism, dihydroclavaminate remains in the active site as a new iron−oxygen species is generated from second equivalents of α-KG and O_2. Hydrogen abstraction is then proposed to occur at C-3 to form a carbon-centered radical, leading to desaturation of dihydroclavaminate to clavaminate.[20]

In the absence of substrates, an uncoupled reaction occurs in which α-KG is decarboxylated, but the reactive iron−oxygen species is quenched by water to give hydrogen peroxide and inactive CS enzyme.[15] The uncoupled reaction occurs in many of the α-KG-dependent enzymes and proceeds at rates significantly below those of normal substrate turnover (1−6%).[7,27−32] Because this inactivation may also occur a fraction of the time in the presence of substrate (∼1 in 890 turnovers for CS2[33]), many α-KG-dependent enzymes require substoichiometric amounts of ascorbate to reactivate the enzyme for catalysis.[23,34] From a mechanistic view, the uncoupled reaction in CS2 argues

(11) Baldwin, J. E.; Lloyd, M. D.; Wha-Son, B.; Schofield, C. J.; Elson, S. W.; Baggaley, K. H.; Nicholson, N. H. *J. Chem. Soc., Chem. Commun.* **1993**, 500−502.
(12) Elson, S. W.; Baggaley, K. H.; Gillett, J.; Holland, S.; Nicholson, N. H.; Sime, J. T.; Woroniecki, S. R. *J. Chem. Soc., Chem. Commun.* **1987**, 1736−1740.
(13) Krol, W. J.; Basak, A.; Salowe, S. P.; Townsend, C. A. *J. Am. Chem. Soc.* **1989**, *111*, 7625−7627.
(14) Baldwin, J. E.; Bradley, M. *Chem. Rev. (Washington, D.C.)* **1990**, *90*, 1079−1088.
(15) Salowe, S. P.; Marsh, E. N.; Townsend, C. A. *Biochemistry* **1990**, *29*, 6499−6508.
(16) Marsh, E. N.; Chang, M. D.-T.; Townsend, C. A. *Biochemistry* **1992**, *31*, 12648−12657.
(17) Lawlor, E. J.; Elson, S. W.; Holland, S.; Cassels, R.; Hodgson, J. E.; Lloyd, M. D.; Baldwin, J. E.; Schofield, C. J. *Tetrahedron* **1994**, *50*, 8737−8748.
(18) Busby, R. W.; Chang, M. D.-T.; Busby, R. C.; Wimp, J.; Townsend, C. A. *J. Biol. Chem.* **1995**, *270*, 4262−4269.
(19) Ward, J. M.; Hodgson, J. E. *FEMS Microbiol. Lett.* **1993**, *110*, 239−242.
(20) Salowe, S. P.; Krol, W. J.; Iwata-Reuyl, D.; Townsend, C. A. *Biochemistry* **1991**, *30*, 2281−2292.
(21) Siegel, B. *Bioorg. Chem.* **1979**, *8*, 219−226.
(22) Myllylä, R.; Tuderman, L.; Kivirikko, K. I. *Eur. J. Biochem.* **1977**, *80*, 349−357.
(23) Kivirikko, K. I.; Myllylä, R.; Pihlajaniemi, T. *FASEB J.* **1989**, *3*, 1609−1617.
(24) Basak, A.; Salowe, S. P.; Townsend, C. A. *J. Am. Chem. Soc.* **1990**, *112*, 1654−1656.
(25) Townsend, C. A.; Basak, A. *Tetrahedron* **1991**, *47*, 2591−2602.
(26) Roach, P. L.; Clifton, I. J.; Hensgens, C. M. H.; Shibata, N.; Schofield, C. J.; Hajdu, J.; Baldwin, J. E. *Nature* **1997**, *387*, 827−830.
(27) Tuderman, L.; Myllylä, R.; Kivirikko, K. I. *Eur. J. Biochem.* **1977**, *80*, 341−348.
(28) Puistola, U.; Turpeenniemi-Hujanen, T. M.; Myllylä, R.; Kivirikko, K. I. *Biochim. Biophys. Acta* **1980**, *611*, 40−50.
(29) Holme, E.; Lindstedt, S. *Biochim. Biophys. Acta* **1982**, *704*, 278−283.
(30) Wehbie, R. S.; Punekar, N. S.; Lardy, H. A. *Biochemistry* **1988**, *27*, 2222−2228.
(31) Hsu, C.-A.; Saewert, M. D.; Polsinelli, L. F., Jr.; Abbott, M. T. *J. Biol. Chem.* **1981**, *256*, 6098−6101.
(32) Holme, E.; Lindstedt, S.; Nordin, I. *Biochem. Biophys. Res. Commun.* **1982**, *107*, 518−524.
(33) This rate of inactivation is a revision of the original literature (ref 15) based on the corrected molecular mass of CS2.
(34) Myllylä, R.; Majamaa, K.; Günzler, V.; Hanauske-Abel, H. M.; Kivirikko, K. I. *J. Biol. Chem.* **1984**, *259*, 5403−5405.

for the presence of an {Fe}CS2−α-KG−O_2 complex and supports the formation of the reactive iron−oxygen species prior to the oxidation of proclavaminate.

Recent studies have shown that a single ferrous active site is responsible for all three reactions catalyzed by CS2, with the stoichiometric requirement of one Fe^{2+} per enzyme molecule ($K_m \approx 1$ μM).[35] Addition of α-KG to the enzyme with Fe^{2+} and ascorbate under assay conditions causes rapid inactivation ($t_{1/2} \approx 5$ min vs $t_{1/2} > 8$ h for the apoenzyme) as the uncoupled reaction occurs.[20] Co^{2+} is found to bind tightly to CS2 in a competitive manner with Fe^{2+}, producing catalytically inactive enzyme which is protected against oxidative self-inactivation in the presence of α-KG and O_2.[18] Chemical modifications with diethyl pyrocarbonate and *N*-ethylmaleimide on {Co^{2+}}CS2 are consistent with the presence of histidine and cysteine residues at or near the active site.[18] These results are similar to site-directed mutagenesis experiments on human prolyl 4-hydroxylase[36] and IPNS[37] which implicate two histidines and one aspartate as critical iron-binding residues. However, to date there are no crystal structures and virtually no direct information about the Fe^{2+} coordination sphere for CS2 or any α-KG-dependent enzyme.

Non-heme ferrous sites have been difficult to study by spectroscopic means as these non-Kramers ions lack strong absorption features and are generally EPR silent. We have developed a protocol that utilizes magnetic circular dichroism (MCD) and variable-temperature, variable-field (VTVH) MCD spectroscopies to probe the geometric and electronic structure of high-spin $S = 2$ Fe^{2+} centers.[38,39] The ^5D ground state for d^6 Fe^{2+} is split under octahedral symmetry into a $^5T_{2g}$ ground state (corresponding to d_{yz}, d_{xz}, d_{xy}) and a ^5E_g excited state ($d_{x^2-y^2}$, d_{z^2}), separated by $10Dq \approx 10\,000$ cm^{-1} for O and N ligands. Near-IR (NIR) MCD spectroscopy allows the direct observation of the d → d transitions, and the splitting of the ^5E_g excited state ($\Delta^5E_g \equiv d_{x^2-y^2} - d_{z^2}$) is sensitive to the coordination number and geometry of the site. In general, six-coordinate distorted octahedral Fe^{2+} sites show two transitions at ∼10 000 cm^{-1}, split by ∼2000 cm^{-1} ($\Delta^5E_g \approx 2000$ cm^{-1}), five-coordinate sites show two transitions at ∼10 000 and ∼5000 cm^{-1} ($\Delta^5E_g \approx 5000$ cm^{-1}), and distorted four-coordinate sites show two transitions in the 4000−7000 cm^{-1} region, where $10Dq(T_d) = (-4/9)10Dq(O_h)$.[39]

VTVH MCD is used to obtain complementary ground-state electronic structure information. The MCD intensity for non-Kramers Fe^{2+} centers shows unusual temperature and field dependence, which is characterized by nested saturation magnetization behavior (i.e., nonsuperimposing isotherms when plotted vs $\beta H/2kT$). For negative zero-field splitting (ZFS) systems ($D < 0$, $M_S = \pm 2$ lowest), this behavior is due to the rhombic zero-field splitting (δ) of the $M_S = \pm 2$ ground state, which shows a nonlinear magnetic field dependence.[40] δ is sensitive to site geometry and is found to be larger, corresponding to more nesting, for six-coordinate ($\delta \approx 4-7$ cm^{-1}) than for five-coordinate sites ($\delta < 4$ cm^{-1}).[39] Ground-state spin Hamiltonian parameters are obtained by numerically fitting experimental VTVH MCD data to an intensity expression which includes δ and $g_{\parallel}$, as well as the transition polarization ratio (M_z/M_{xy}) and contributions from temperature-independent *B*-terms.[39] This analysis has now been extended to include +ZFS systems ($D > 0$, $M_S = 0$ lowest), which can show qualitatively similar VTVH MCD behavior arising from a pseudodoublet ground state composed of the $M_S = 0$ and one component of the $M_S = \pm 1$ sublevels which mix through off-axis Zeeman effects.[41] +ZFS systems can be distinguished from −ZFS by a large ground-state splitting (∼D instead of δ) and the presence of an additional MCD-inactive low-lying singlet excited state, which is the other component of $M_S = \pm 1$.

The ground-state spin Hamiltonian parameters are directly related to the splitting of the $^5T_{2g}$ state ($\Delta \equiv d_{xz,yz} - d_{xy}$ and $V \equiv d_{xz} - d_{yz}$) for six- and five-coordinate sites and allows one to determine the t_{2g} orbital energies, which are sensitive to π-bonding interactions.[39] The larger δ values found for six-coordinate sites are associated with smaller values of Δ, and conversely, small δ values are associated with larger Δ values for five-coordinate sites due to the open coordination position. Combined, NIR MCD and VTVH MCD provide a complete description of the d orbitals for a given Fe^{2+} site, which can be used to probe oxygen and substrate reactivity and to obtain mechanistic insight on a molecular level for non-heme iron enzymes.[40,42−46]

We now apply these techniques to directly probe the ferrous active site in resting CS2 and its interaction with α-KG cosubstrate. Circular dichroism (CD) titrations have been performed to investigate Fe^{2+} binding to CS2, both without and with cosubstrate, as well as α-KG binding to the apoenzyme and iron-containing enzyme. Ligand field CD, MCD, and VTVH MCD have been used to obtain information about the active-site coordination number and geometry in the resting enzyme and to probe changes at the active site due to the presence of α-KG. During these studies, it was observed that addition of α-KG to the colorless iron-containing enzyme produced a pink color, indicating the presence of charge-transfer transitions. UV/vis absorption, CD, and MCD spectroscopies have been used to further investigate the charge-transfer transitions in order to probe the Fe^{2+}−α-KG interaction. These results offer the first direct information about the ferrous active site in CS2 and the interplay with cosubstrate which provides insight into the catalytic mechanism.

Experimental Section

Isolation of Clavaminate Synthase. The isozyme CS2 was overexpressed and purified according to published procedures[18] with the following modifications. The EDTA and phenylmethylsulfonyl fluoride (PMSF) concentrations were increased in each buffer as specified below. The glycerol concentration in all buffers was decreased from 20% to 10%, and the buffers were thoroughly degassed under nitrogen prior to use. CS2 purification was carried out on 40 g of *E. coli* JM101 cell paste and the concentration of additives (lysozyme and Brij 58) adjusted accordingly. A fresh 2 mL solution of 100 mM

(35) Busby, R. W.; Townsend, C. A. *Bioorg. Med. Chem.* **1996**, *4*, 1059−1064.
(36) Myllyharju, J.; Kivirikko, K. I. *EMBO J.* **1997**, *16*, 1173−1180.
(37) Borovok, I.; Landman, O.; Kreisberg-Zakarin, R.; Aharonowitz, Y.; Cohen, G. *Biochemistry* **1996**, *35*, 1981−1987.
(38) Solomon, E. I.; Zhang, Y. *Acc. Chem. Res* **1992**, *25*, 343−352.
(39) Solomon, E. I.; Pavel, E. G.; Loeb, K. E.; Campochiaro, C. *Coord. Chem. Rev.* **1995**, *144*, 369−460.
(40) Whittaker, J. W.; Solomon, E. I. *J. Am. Chem. Soc.* **1988**, *110*, 5329−5339.
(41) Campochiaro, C.; Pavel, E. G.; Solomon, E. I. *Inorg. Chem.* **1995**, *34*, 4669−4675.
(42) Loeb, K. E.; Westre, T. E.; Kappock, T. J.; Mitić, N.; Glasfeld, E.; Caradonna, J. P.; Hedman, B.; Hodgson, K. O.; Solomon, E. I. *J. Am. Chem. Soc.* **1997**, *119*, 1901−1915.
(43) Pavlosky, M. A.; Zhang, Y.; Westre, T. E.; Gan, Q.-F.; Pavel, E. G.; Campochiaro, C.; Hedman, B.; Hodgson, K. O.; Solomon, E. I. *J. Am. Chem. Soc.* **1995**, *117*, 4316−4327.
(44) Loeb, K. E.; Zaleski, J. M.; Westre, T. E.; Guajardo, R. J.; Mascharak, P. K.; Hedman, B.; Hodgson, K. O.; Solomon, E. I. *J. Am. Chem. Soc.* **1995**, *117*, 4545−4561.
(45) Pavel, E. G.; Martins, L. J.; Ellis, W. R., Jr.; Solomon, E. I. *Chem. Biol.* **1994**, *1*, 173−183.
(46) Mabrouk, P. A.; Orville, A. M.; Lipscomb, J. D.; Solomon, E. I. *J. Am. Chem. Soc.* **1991**, *113*, 4053−4061.

PMSF in 2-propanol was added to the lysis buffer prior to use to prevent proteolytic protein degradation, and the concentration of EDTA was increased from 10 μM to 2 mM. Once the cell-free extract was prepared, a 40-μL solution of a 10 mg/mL DNase I solution was added. Soy trypsin inhibitor was added (500 μL of 5 mg/mL solution) to the diluted cell-free extract prior to streptomycin sulfate precipitation. Following the ammonium sulfate fractionation, the protein pellet was resuspended in 20 mL of 50 mM Tris buffer (pH 7.0) containing 1 mM dithiothreitol (DTT), 1 mM benzamidine, 400 μM PMSF, and 200 μM EDTA. The protein was dialyzed for 2 h against 2000 mL of this buffer, followed by overnight dialysis against an equal volume. The dialyzed protein was removed and diluted to 100 mL with Tris-EDTA buffer containing 100 μM EDTA, 1 mM DTT, 1 mM benzamidine, and 200 μM PMSF. A 1000-mL linear gradient of KCl from 0 to 400 mM was used to elute CS2. Gel filtration chromatography was accomplished using Tris-EDTA buffer containing 50 μM EDTA, 1 mM DTT, 1 mM benzamidine, and 100 μM PMSF. The active fractions were pooled and concentrated, and the homogeneous apoenzyme was stored in 50 mM MOPS buffer, pD 7, with 1 mM DTT and 10% glycerol-d_3 to stabilize the protein, and kept frozen at −86 °C until used for spectroscopy.

Preparation of Samples for Spectroscopy. All commercial reagents were used without further purification: MOPS buffer (Sigma), D_2O (99.9 atom % D; Aldrich), sodium deuterioxide (99+ atom % D; Sigma), glycerol-d_3 (98 atom % D; Cambridge Isotopes Laboratory), 2-oxopentanedioic acid (α-ketoglutaric acid, or 2-oxoglutaric acid; Sigma), ferrous ammonium sulfate (FeAS, $[Fe(H_2O)_6](NH_4)_2(SO_4)_2$; MCB Manufacturing Chemists, Inc.). Samples for spectroscopy were prepared under an inert atmosphere inside a N_2-purged wet box. ApoCS2 was made anaerobic by purging a vial of the apoenzyme with argon gas on a Schlenk line and alternating quick cycles of vacuum and argon. Fe^{2+} was added in microliter quantities to apoCS2 from anaerobic stock solutions of FeAS in degassed MOPS buffer, pD 7. α-KG stock solutions were prepared in D_2O, adjusted to pD 7 by the addition of 40 wt % NaOD, and thoroughly degassed before addition in microliter quantities to the enzyme. Fresh stock solutions of FeAS and α-KG were prepared for each set of experiments. Wherever possible, parallel samples of resting CS2 and CS2+α-KG were prepared simultaneously. Unless otherwise noted, iron-containing CS2 samples contain 0.8 equiv of Fe^{2+} relative to apoenzyme (20% excess "ligand") and CS2+α-KG samples contain 15× α-KG relative to apoenzyme.

Samples for absorption and CD spectroscopy (2.5−4.7 mM apoCS2) were kept anaerobic by using a custom-made 0.5-cm path length masked optical cell (Wilmad) fitted with a gastight Teflon stopcock (LabGlass). Titration additions into the anaerobic optical cell were carried out in the wet box using gastight syringes fitted with custom 5-in.-long needles (Hamilton Co.); volumes were adjusted to account for solution contained within the needle. Samples for MCD spectroscopy (1.5−2.3 mM apoCS2) were prepared by the anaerobic addition of FeAS to apoenzyme, followed by addition of α-KG where appropriate, and 50−65 vol % of degassed glycerol-d_3. A pale pink color was observed when α-KG was added to the colorless iron-containing enzyme or if FeAS was added to the colorless apoCS2+α-KG solution. MCD samples were injected into a cell assembled under N_2 with a 0.3-cm-thick neoprene gasket sandwiched between two infrasil quartz disks and secured between copper plates; cells were frozen under liquid N_2 immediately upon removal from the wet box. Control samples of FeAS, α-KG, and FeAS+α-KG (in MOPS (pD 7) or MOPS/glycerol-d_3) were prepared under identical conditions to those of the protein samples.

Instrumentation. Room-temperature UV/vis (190−820 nm) electronic absorption spectra were recorded on an HP 8452A diode array spectrophotometer. UV/vis (300−850 nm) CD and MCD spectra were obtained using a Jasco J500C spectropolarimeter with an extended S-20 photomultiplier tube (Hammamatsu) and equipped with an Oxford Instruments SM4-7T magnet/cryostat capable of fields up to 7 T and temperatures from 1.6 to 100 K. NIR (600−2000 nm) CD and MCD spectra were recorded on a Jasco J200D spectropolarimeter with a liquid N_2-cooled InSb detector and an Oxford Instruments SM4000-7T superconducting magnet/cryostat (0−7 T, 1.6−100 K).

CD samples were maintained at a temperature of 278 K using a recirculating water bath and thermostated cell holder on each spectropolarimeter so that data for a single sample could be collected in both the UV/vis and NIR regions. CD spectra are baseline corrected by subtracting the buffer and cell backgrounds from the raw data. Depolarization of frozen MCD samples was judged to be <5% by comparing the CD spectra of a nickel (+)-tartrate solution placed before and after the sample. MCD spectra are corrected for the natural CD and zero-field baseline effects due to the optical quality of the frozen sample by subtracting the corresponding 0 T scan at each temperature. In some cases, in particular the VTVH MCD data, the reported MCD data are the averaged subtraction of the negative field raw data (collected with the magnetic poles reversed) from the positive field raw data so as to avoid subtraction problems due to shifting baselines in poor quality frozen glasses.

Fitting Procedures. Spectra were fit to Gaussian band shapes using a modified Levenberg−Marquardt constrained nonlinear least-squares fitting routine. In the case of simultaneous fitting of CD, MCD, and absorption spectra, the intensities were allowed to vary, keeping the transition energies fixed wherever possible and allowing for slight broadening of the half-width at half-maximum (HWHM) values upon going from low-temperature (5 K) MCD to room-temperature (278 K) CD and absorption spectra. Saturation magnetization data were normalized to the maximum observed intensity and fit according to published procedures to extract ground-state parameters.[39] Both the negative and positive ZFS models were applied to the VTVH MCD data in determining the best fit. Binding constants were estimated from CD titration data using the method of Rose and Drago.[47,48]

Density Functional Calculations. Calculations were performed using versions 1.1.3 and 2.0.1 of the commercially available Amsterdam Density Functional (ADF) programs by Baerends and co-workers.[49] The Vosko−Wilk−Nusair local density approximation[50] was used for the exchange and correlation energy; Becke[51] and Perdew[52] nonlocal gradient corrections for exchange and correlation were included. Atomic basis functions, core expansion functions, core coefficients, and fit functions were used as provided by database IV, including Slater-type orbital triple-ζ basis sets, with all core levels treated as frozen orbitals. Numerical integration was set to 6.0 and convergence was accepted when the maximum element in the error matrix was less than 10^{-6}.

Results and Analysis

A. Iron and α-Ketoglutarate Binding. CD spectroscopy has been used to probe Fe^{2+} and α-KG binding to CS2 and to obtain approximate binding constants. Figure 1A (light dotted line) shows the featureless UV/vis CD spectrum of apoCS2 prior to any additions. Addition of α-KG to apoCS2 causes the appearance of a single band at 29 000 cm^{-1}, assigned as an n → π^* transition (vide infra), which grows with increasing aliquots of α-KG, as shown in Figure 1A (solid lines). This feature does not saturate at stoichiometric amounts of α-KG, but continues to increase up to 15 equiv, from which an estimated binding constant of $K_B \approx 200-500$ M^{-1} is obtained for α-KG binding to apoCS2.

The NIR region CD spectrum of the apoenzyme is shown in Figure 1B (dotted line) and is also featureless. Addition of Fe^{2+} results in a broad positive band at ∼8500 cm^{-1} in the CD spectrum which increases up to stoichiometric amounts of iron (Figure 1B, solid lines) and which corresponds to the d → d ligand field transitions for a ferrous site. Since both the apoenzyme and aqueous FeAS are CD-silent and the ∼8500 cm^{-1} band ceases to increase above stoichiometric equivalents of Fe^{2+} (not shown for clarity), these d → d transitions must be

(47) Connors, K. A. *Binding Constants: The Measurement of Molecular Complex Stability*; John Wiley & Sons: New York, 1987; Chapter 4.
(48) Rose, N. J.; Drago, R. S. *J. Am. Chem. Soc.* **1959**, *81*, 6138−6141.
(49) te Velde, G.; Baerends, E. J. *J. Comput. Phys.* **1992**, *99*, 84−98.
(50) Vosko, S. H.; Wilk, L.; Nusair, M. *Can. J. Phys.* **1980**, *58*, 1200−1211.
(51) Becke, A. D. *Phys. Rev. A* **1988**, *38*, 3098−3100.
(52) Perdew, J. P.; Wang, Y. *Phys. Rev. B* **1986**, *33*, 8800−8802.

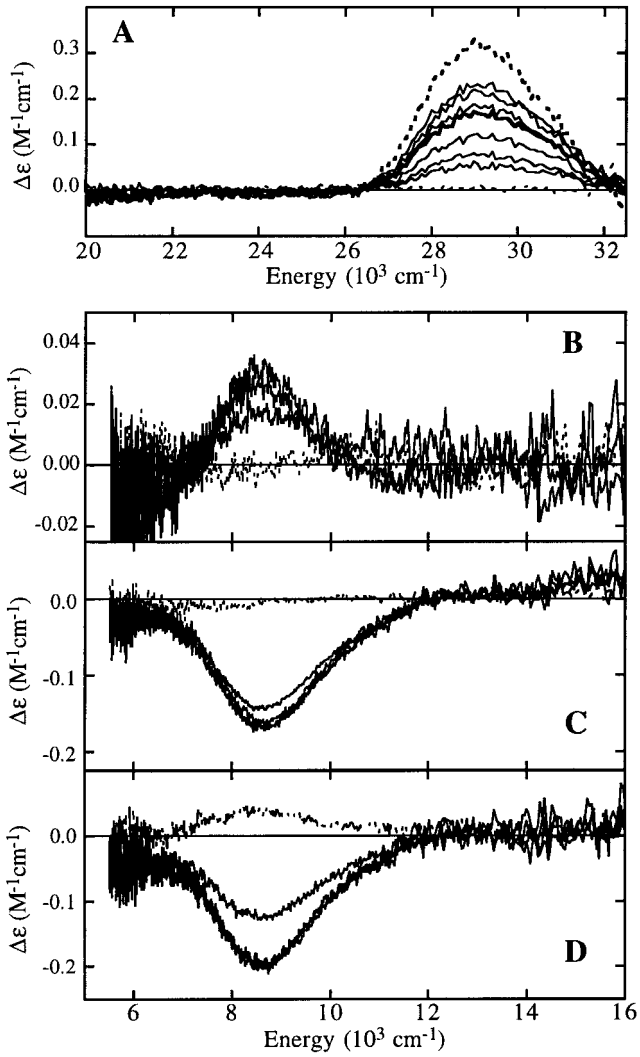

Figure 1. Titration of apoCS2 with Fe^{2+} and α-KG. (A) Charge-transfer CD spectra at 278 K of apoCS2 (light dotted line) with 0.25, 0.5, 0.75, 1.0 (heavy solid line), 1.25, 1.5, 1.75, and ~15 (heavy dotted line) equiv of α-KG. (B) Ligand field CD spectra at 278 K of apoCS2 (dotted line) with 0.5, 0.75, and 1.0 (heavy solid line) equiv of Fe^{2+}; the spectrum with 1.25 equiv of Fe^{2+} superimposes on that with 1.0 equiv and has been omitted for clarity. (C) CD spectra at 278 K of apoCS2 + 15× α-KG (dotted line) with 0.5, 0.75, 1.0, and 1.5 equiv of Fe^{2+} relative to apoCS2. (D) CD spectra at 278 K of apoCS2 + 0.8× Fe^{2+} (dashed line) with 0.5, 0.75, 1.0, and 15 equiv of α-KG relative to Fe^{2+}. $\Delta\epsilon$ values reported are per concentration of apoenzyme in A−C and per concentration of iron-bound CS2 in D.

due to iron in the protein active site. From these data, a binding constant for Fe^{2+} binding to the apoenzyme is estimated as $K_B > 5000\ M^{-1}$. Figure 1C (dotted line) presents the CD spectrum of apoCS2 + 15× α-KG (denoted apoCS2+α-KG), which shows no features in the ligand field region. When Fe^{2+} is added, a broad negative band associated with the ferrous ligand field d → d transitions appears. As with the resting enzyme, this CD feature saturates at stoichiometric equivalents of Fe^{2+} (Figure 1C, solid lines). Additionally, control studies show that aqueous FeAS, aqueous α-KG, and FeAS + 15× α-KG in MOPS buffer, pD 7, are all CD-silent so that the negative band seen in Figure 1C must arise from iron in the active site of a CS2+α-KG complex. The binding constant estimated from these data for Fe^{2+} binding to apoCS2+α-KG is $K_B > 10\,000\ M^{-1}$. These results show that iron is tightly bound to the protein, both in the resting enzyme and the enzyme + cosubstrate complex, which is consistent with kinetic studies on CS2 that show $K_m(Fe^{2+}) = 1-2\ \mu M$.[15] Further analysis of the ligand field CD transitions for resting CS2 and CS2+α-KG is presented in the next section.

To probe α-KG binding to resting CS2 (i.e., with Fe^{2+} present), a titration was performed in which increasing amounts of α-KG were added to CS2 + 0.8 equiv Fe^{2+}. The CD spectrum of the resting CS2 sample is shown in Figure 1D (dashed line) and has the broad positive feature associated with this species. Upon addition of 0.5× α-KG, the positive band disappears and a negative band appears which increases up to stoichiometric amounts of α-KG (Figure 1D, solid lines). This negative feature is identical with that in the spectrum obtained when Fe^{2+} is added to apoCS2+α-KG (Figure 1C), demonstrating that the order of iron or cosubstrate addition is inconsequential in the formation of the CS2+α-KG complex. Additionally, the signal does not increase between 1 equiv and 15 equiv α-KG, as shown in Figure 1D, indicating that cosubstrate is tightly bound. A binding constant for α-KG binding to resting CS2 is estimated as $K_B > 5000\ M^{-1}$, which is an order of magnitude greater than that for α-KG binding to the apoenzyme. Therefore it appears that the presence of Fe^{2+} in the protein facilitates cosubstrate binding, and the high affinity of Fe^{2+} to the active site combined with the high affinity of α-KG to Fe^{2+} [53] indicates that α-KG may migrate to the active site when the metal is present.

B. Ligand Field Region. 1. Resting CS2. The NIR CD, MCD, and VTVH MCD data for resting CS2 are shown in Figure 2, and the excited-state transition energies, ground-state splittings, and ligand field parameters are summarized in Table 1. The 278 K CD spectrum shown in Figure 2A has been Gaussian-resolved into two positive bands (dashed lines) centered at 8730 and 10 740 cm^{-1}. The position of these transitions is consistent with a distorted six-coordinate ferrous site for the resting enzyme. The CD spectrum remains unchanged when the glycerol content is increased from 8−10% (required to stabilize the enzyme) to 60% glycerol-d_3 (not shown for clarity); therefore glycerol-d_3 does not alter the structure of the iron site and may be used as a glassing agent for low-temperature spectroscopy.

The 5 K, 7 T MCD spectrum of resting CS2 is presented in Figure 2B and contains two positive features which have been Gaussian-resolved into bands at 9210 and 10 900 cm^{-1} to give $\Delta^5E_g = 1690\ cm^{-1}$ (see Table 1), indicative again of a distorted six-coordinate ferrous site. Because the energies of d → d transitions are shifted in the MCD relative to those in CD, control studies were performed to verify that iron had not fallen out of the active site during freezing. The low-temperature MCD spectrum of FeAS in MOPS/glycerol-d_3 shows features similar in energy to those seen for resting CS2,[54] as might be expected since FeAS has six waters bound to Fe^{2+} in a distorted octahedral geometry.[55] However, the MCD features for FeAS are three times less intense than those observed for the protein, so that even if all of the iron were displaced from the enzyme active site, it could not account for the intensity seen for resting CS2. Thus the MCD features in Figure 2B are due to iron in the protein active site and the shift in the band energies between the room-temperature CD and low-temperature MCD, which have been reproduced over several different enzyme preparations, are due to the temperature change.

(53) Titration studies monitoring the absorption at 440 nm show that α-KG forms a 1:1 complex with FeAS under conditions used for the enzyme samples and K_B(α-KG) = 2400 ± 200 M^{-1}.

(54) Pavel, E. G.; Solomon, E. I. Unpublished results.

(55) Montgomery, H.; Chastain, R. V.; Natt, J. J.; Witkowska, A. M.; Lingafelter, E. C. *Acta Crystallogr.* **1967**, *22*, 775−780.

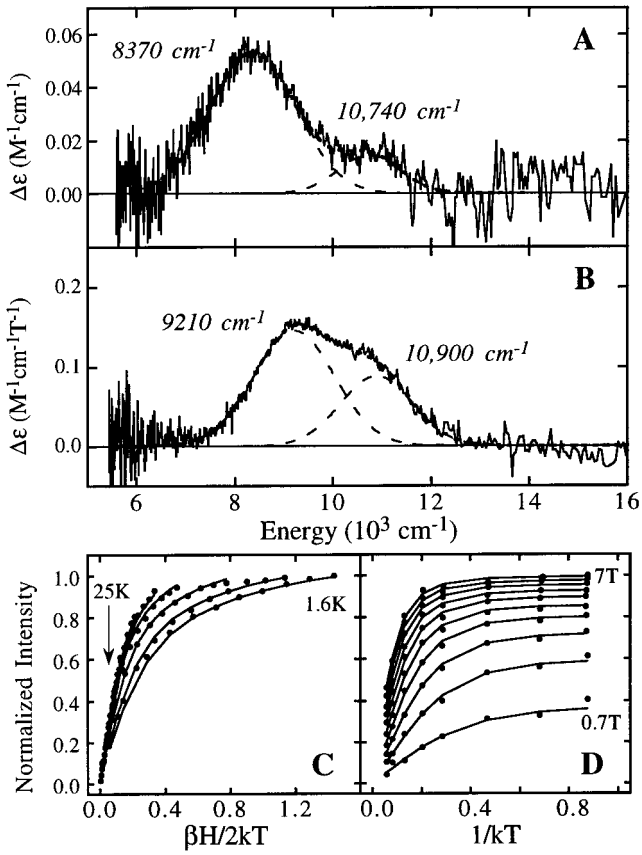

Figure 2. Ligand field CD, MCD, and VTVH MCD data for resting CS2. (A) CD spectrum at 278 K of resting CS2. (B) MCD spectrum at 5 K and 7 T of resting CS2. Plots A and B include Gaussian fits to the data (—) and the individual components (- - -). (C and D) VTVH saturation magnetization behavior of resting CS2 recorded at 9200 cm^{-1}. The normalized data (•) are plotted vs $\beta H/2kT$ (C) for a series of fixed temperatures (1.6, 2, 3, 5, 7, 11, 18, and 25 K) and vs $1/kT$ (D) for a series of fixed fields (0.7−7.0 T in 0.7 T increments). Errors in the intensities are approximately the size of the symbol used and have been omitted for clarity. The best fit (solid lines) to the data was generated by the parameters described in Table 1.

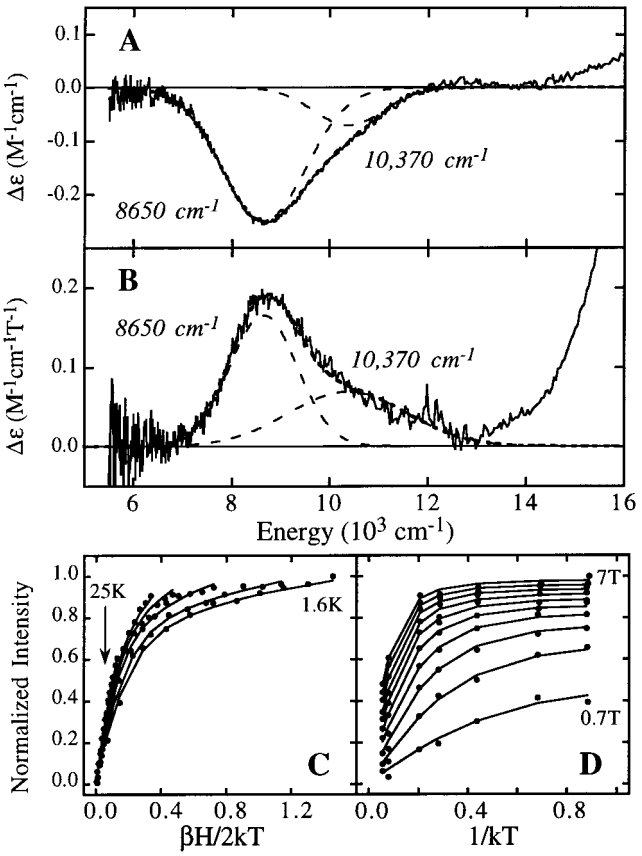

Figure 3. Ligand field CD, MCD, and VTVH MCD data for CS2 + 15× α-KG. (A) CD spectrum at 278 K of CS2+α-KG. B. MCD spectrum at 5 K and 7 T of CS2+α-KG. Plots A and B show the Gaussian fit to the data (—) and the individual components (- - -). (C and D) VTVH saturation magnetization behavior recorded at 8550 cm^{-1}. The normalized data (•) are plotted vs $\beta H/2kT$ (C) for a series of fixed temperatures (1.6, 2, 3, 5, 7, 18, and 25 K) and vs $1/kT$ (D) for a series of fixed fields (0.7−7.0 T in 0.7 T increments). Errors in the intensities are ∼1.5 times the symbol size used and have been omitted for clarity. The best fit (solid lines) to the data was generated by the parameters described in Table 1.

Table 1. Ligand Field MCD Transition Energies, Ground-State Spin Hamiltonian Parameters, and Ligand Field Parameters

	resting CS2	CS2+α-KG
transitions (HWHM)	9210 cm^{-1} (970 cm^{-1})	8650 cm^{-1} (1000 cm^{-1})
	10 900 cm^{-1} (870 cm^{-1})	10 370 cm^{-1} (840 cm^{-1})
Δ^5E_g	1690 cm^{-1}	1630 cm^{-1}
δ (cm^{-1})	4.5 ± 0.15	2.7± 0.3
$g_{\|\|}$	9.2 ± 0.1	8.7 ± 0.2
M_z/M_{xy}[a]	−0.27	−0.16
B-term[b]	0.8%	1.3%
Δ (cm^{-1})	−400 ± 100	−1000 ± 200
$\|V/2\Delta\|$	0.24	0.33
$\|V\|$ (cm^{-1})	190 ± 50	670 ± 100

[a] For $g_\perp$ fixed at 1.0. [b] Reported as a percentage of the C-term intensity scaling factor (see ref 39).

VTVH MCD was used to probe the ground-state splittings by monitoring the MCD intensity at 9200 cm^{-1} for a series of fixed fields at different fixed temperatures. Figure 2C,D shows these data (symbols) plotted vs $\beta H/2kT$ and vs $1/kT$, along with the best fit (lines) to the data. As seen from these plots, the MCD intensity decreases with increasing temperature, indicative of a high-spin Fe^{2+} center. The saturation magnetization behavior for resting CS2 is well described by the negative ZFS non-Kramers model, and the ground-state spin Hamiltonian parameters obtained from the best fit to the data are $g_{||} = 9.2 \pm 0.1$ and $\delta = 4.5 \pm 0.15$ cm^{-1} (see Table 1). This value of δ is well within the range expected for a distorted six-coordinate site. On the basis of these parameters, the $^5T_{2g}$ splittings are determined to be $\Delta \approx -400$ cm^{-1} and $|V| \approx 190$ cm^{-1}. Thus from the CD, MCD, and VTVH MCD data, resting CS2 contains a high-spin ferrous active site with a six-coordinate distorted octahedral geometry.

2. CS2+α-KG Cosubstrate. To investigate the interaction of α-KG with the resting enzyme, CD, MCD, and VTVH MCD were applied to CS2 + 15× α-KG (denoted CS2+α-KG). Although the titration results show that α-KG binds stoichiometrically to resting CS2, a 15-fold excess of cosubstrate was used for the spectroscopy samples to ensure that no residual resting CS2 remained. The 278 K CD of CS2+α-KG is given in Figure 3A and has been Gaussian-resolved into two negative bands at 8650 and 10 370 cm^{-1} indicative of a six-coordinate iron site. The CD spectrum of an analogous FeAS+α-KG sample (i.e., without protein) is featureless; therefore, these two bands are assigned as the ferrous d → d ligand field transitions in the enzyme + cosubstrate complex. This CD spectrum is markedly different than that of the resting enzyme (Figure 2A) in that the sign of the ligand field transitions has reversed and the intensity is much greater for CS2+α-KG. These changes indicate that the geometric environment of the six-coordinate

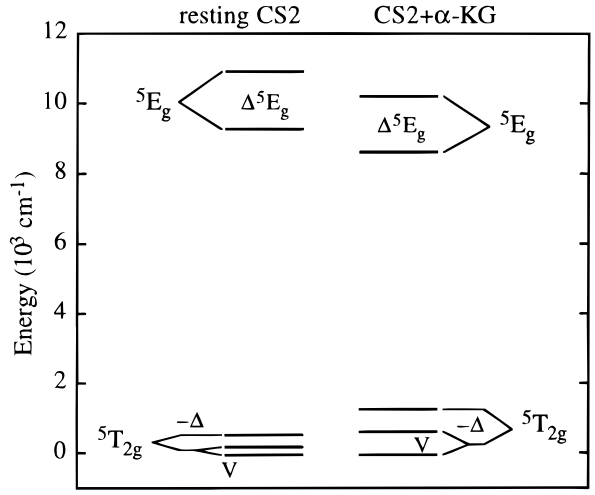

Figure 4. Experimental d-orbital energies for resting CS2 (left) and CS2+α-KG (right) from the ligand field parameters in Table 1.

active site in the resting enzyme has been significantly perturbed by the addition of cosubstrate.

The CD spectrum of CS2+α-KG is unchanged by increasing the glycerol-d_3 content from 8−10% to 60%, so glycerol may be used as a low-temperature glassing agent. The 5 K, 7 T MCD spectrum for CS2+α-KG is shown in Figure 3B and is Gaussian-resolved into two positive bands at 8650 and 10 370 cm^{-1}, the same energies as in the CD spectrum, to give Δ^5E_g = 1630 cm^{-1} (see Table 1). This excited-state splitting supports the assignment of a distorted six-coordinate active site in CS2+α-KG. The MCD d → d transitions in CS2+α-KG (10*Dq* = 9500 cm^{-1}) are shifted to lower energy relative to those in resting CS2 (10*Dq* = 10 050 cm^{-1}), indicating that the six-coordinate ferrous sites are different. Furthermore, the lower value of 10*Dq* indicates an overall weaker ligand field at the Fe^{2+} site in the enzyme + cosubstrate complex.

Figure 3C,D shows the VTVH MCD data (symbols) observed for CS2+α-KG at 8550 cm^{-1} and the best fit (lines) to the data. The saturation magnetization behavior is well-described by the negative ZFS non-Kramers doublet model, and the ground-state spin Hamiltonian parameters obtained from the fit are $g_{||} = 8.7 \pm 0.2$ and $\delta = 2.7 \pm 0.3$ cm^{-1}. Application of the $^5T_{2g}$ analysis gives splitting parameters of $\Delta \approx -1000$ cm^{-1} and $|V| \approx 670$ cm^{-1} (see Table 1). The saturation magnetization behavior observed for CS2+α-KG is different than that of resting CS2 as seen by the differences in the fits, particularly the smaller value of δ in the enzyme + cosubstrate complex (2.7 ± 0.3 cm^{-1} vs 4.5 ± 0.15 cm^{-1}). In fact, this value of δ is less than would be expected for a six-coordinate ferrous center and corresponds to a larger splitting of the t_{2g} d orbitals (Δ), indicating that α-KG not only perturbs the active site in CS2, but is involved in π-bonding interactions with the metal. The experimentally determined d-orbital energy level diagram for CS2+α-KG is compared to that of resting CS2 in Figure 4, which shows the weaker ligand field in the presence of cosubstrate and the larger splitting of the t_{2g} orbitals for CS2+α-KG, indicative of Fe−α-KG π interactions.

C. Charge-Transfer Region. The ligand field MCD spectrum of CS2+α-KG shows the tail of a third band to higher energy (Figure 3B), indicating the possibility of low-lying charge-transfer transitions. To probe this further, UV/vis absorption, CD, and MCD were applied to the apoenzyme and the iron-containing enzyme, both with and without α-KG. These data are summarized in Figure 5 and the transition energies in Table 2. The apoenzyme is essentially featureless

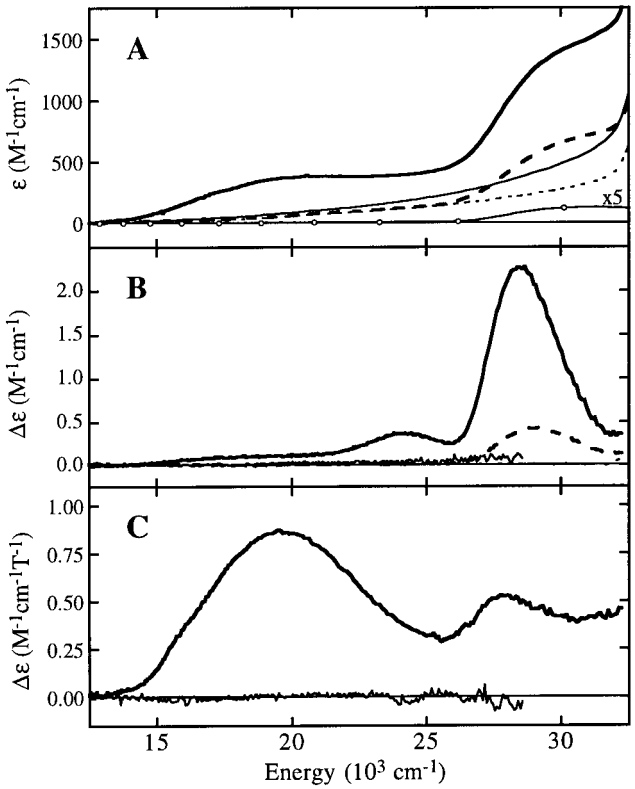

Figure 5. Charge-transfer absorption, CD, and MCD spectra of apoenzyme ± α-KG, CS2 ± α-KG, and aqueous α-KG. (A) Room-temperature absorption spectra of apoCS2 (light dashed line), apoCS2+α-KG (heavy dashed line), resting CS2 (light solid line), CS2+α-KG (heavy solid line), and α-KG in MOPS, pD 7 (−∘−). The absorption spectrum of aqueous α-KG has been multiplied by 5. (B) CD spectra at 278 K of apoCS2 (light dashed line, coincident with the zero line), apoCS2+α-KG (heavy dashed line), CS2 (light solid line), CS2+α-KG (heavy solid line). (C) MCD spectra at 5 K and 7 T of CS2 (light solid line) and CS2+α-KG (heavy solid line). CD and MCD spectra for resting CS2 cut off at ∼350 nm due to sample problems and poor optical glasses. Enzyme samples contain 0.6 (Abs) or 0.8 (CD/MCD) equiv Fe^{2+}; all α-KG-containing enzyme samples contain 15× α-KG relative to apoCS2.

Table 2. Charge-Transfer Transition Energies (cm^{-1}) of Aqueous α-KG, ApoCS2+α-KG, CS2+α-KG, and FeAS+α-KG

		MLCT transitions			n → π^*
complex	technique	band 1	band 2	band 3	transition
α-KG in MOPS	Abs				31 500
apoCS2+α-KG	CD				29 000
CS2+α-KG	Abs/CD	17 820	20 800	24 070	28 500
	MCD	17 820	20 800	24 070	27 900
	(HWHM)	(2050)	(2070)	(1720)	(1670)
FeAS+α-KG	Abs/MCD	∼22 500 (broad)			30 500

in the charge-transfer region, showing only a slight tail in the room-temperature absorption spectrum (Figure 5A, light dashed line) and no features whatsoever in the 278 K CD spectrum (Figure 5B, light dashed line, nearly coincident with the zero line). With the addition of iron, resting CS2 is likewise featureless in absorption and CD (light solid lines in Figure 5A,B), as well as in the 5 K, 7 T MCD spectrum (Figure 5C). Thus there are no charge-transfer transitions due to the apoprotein or resting CS2 in the absence of cosubstrate.

The room-temperature absorption of aqueous α-KG in MOPS buffer, pD 7, is presented as the marked line in Figure 5A and shows a single weak band at ∼31 500 cm^{-1} ($\epsilon \approx 26$ M^{-1} cm^{-1}). This feature is analogous to the weak n → π^* transitions

observed in α,β-dicarbonyl compounds[56] and is assigned as the transition from the highest occupied molecular orbital (HOMO) (denoted "n") to the π^* lowest unoccupied molecular orbital (LUMO) of the α-keto−carboxylate moiety in α-KG. While the n → π^* transition is seen in absorption, it is not observed in CD, as expected since α-KG is achiral. Addition of 15-fold α-KG to apoCS2 results in the appearance of a new feature above the protein tail in the region of the α-KG n → π^* transition (Figure 5A, heavy dashed line). Because there is excess cosubstrate present, it is difficult to discern if the feature in the apoCS2+α-KG absorption spectrum is shifted relative to the n → π^* transition from aqueous α-KG. However, the CD spectrum of apoCS2+α-KG (Figure 5B, heavy dashed line) clearly shows a single transition at 29 000 cm^{-1} which must be the n → π^* transition arising from α-KG bound to the apoenzyme since α-KG and apoCS2 by themselves are CD-silent in this region. The presence of the α-KG n → π^* transition in the CD spectrum demonstrates that cosubstrate must be in a chiral environment once it has bound to the enzyme.

When Fe^{2+} is added to form the CS2+α-KG complex, a pink color appears and the UV/vis absorption spectrum (Figure 5A, heavy solid line) shows a new low-energy feature at ∼20 000 cm^{-1} ($\epsilon_{500} \approx 375\ M^{-1}\ cm^{-1}$), which can be assigned as a metal-to-ligand charge-transfer (MLCT) transition. There is also an increased absorption in the region of the α-KG n → π^* transition. The 278 K CD spectrum of CS2+α-KG (Figure 5B, heavy solid line) shows a broad low-intensity transition at ∼20 000 cm^{-1} and a higher intensity band at ∼24 000 cm^{-1} which coincide with the pink band in the absorption spectrum. Additionally, the n → π^* transition observed in the CD spectrum has shifted slightly from 29 000 cm^{-1} for α-KG bound to apoCS2 to 28 500 cm^{-1} for α-KG bound to the iron-containing enzyme and has gained significant intensity. What was seen as a tail in the ligand field MCD spectrum of CS2+α-KG is found to be an intense broad feature at ∼20 000 cm^{-1} in the low-temperature MCD spectrum (Figure 5C, heavy solid line), which also shows a second band at ∼28 000 cm^{-1}. These two features display a similar temperature dependence in their MCD intensity, indicating that the intraligand n → π^* transition has become paramagnetic. Quantitative analysis of the charge-transfer VTVH MCD data is precluded by a very large (>10%) temperature-independent B-term overlaying the intrinsic saturation magnetization behavior.

As with the ligand field transitions, it is important to verify that the low-energy charge-transfer transitions observed for CS2+α-KG are due to Fe^{2+} in the enzyme active site. The room-temperature absorption and low-temperature MCD spectra of an FeAS+α-KG control sample are shown in Figure 6A and B (solid lines), respectively, as compared to those of CS2+α-KG (dashed lines). The control sample shows spectral features similar to those of the enzyme + cosubstrate, with one broad low-energy feature and a second band to higher energy. However, the transitions for FeAS+α-KG are shifted by ∼2500 cm^{-1} to higher energy (see Table 2) and the absorption and MCD intensities are much weaker relative to CS2+α-KG. Additionally, while CS2+α-KG shows a rich UV/vis CD spectrum (Figure 5B), FeAS+α-KG is CD-silent throughout this region, confirming that the features seen for CS2+α-KG must be due active site Fe^{2+}.

Figure 7 presents the simultaneous Gaussian resolution of the absorption, CD, and MCD spectra for the CS2+α-KG complex. The lower energy region is resolved into three bands centered at 17 820, 20 800, and 24 070 cm^{-1} (see Table 2). While control studies confirm that these features are due to iron in the enzyme + cosubstrate active site, they also support their

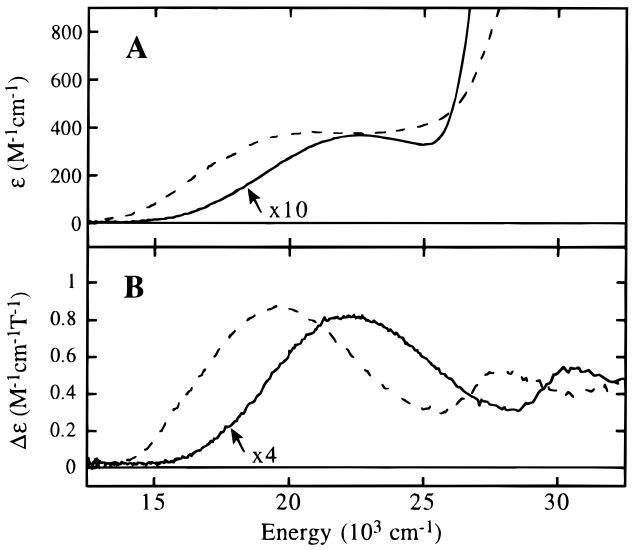

Figure 6. Charge-transfer absorption and MCD spectra of FeAS+α-KG control sample. (A) Room-temperature absorption spectrum of FeAS+α-KG (—) focusing on the MLCT transition region. The data have been multiplied by 10 and compared to that of CS2+α-KG (- - -). (B) 5 K, 7 T MCD spectrum of FeAS+α-KG (—), multiplied by 4 and compared to that of CS2+α-KG (- - -). The control sample for absorption contains FeAS + 15× α-KG in MOPS, pD 7; the MCD sample contains FeAS + 10× α-KG in ∼60% (v/v) glycerol-d_3/MOPS.

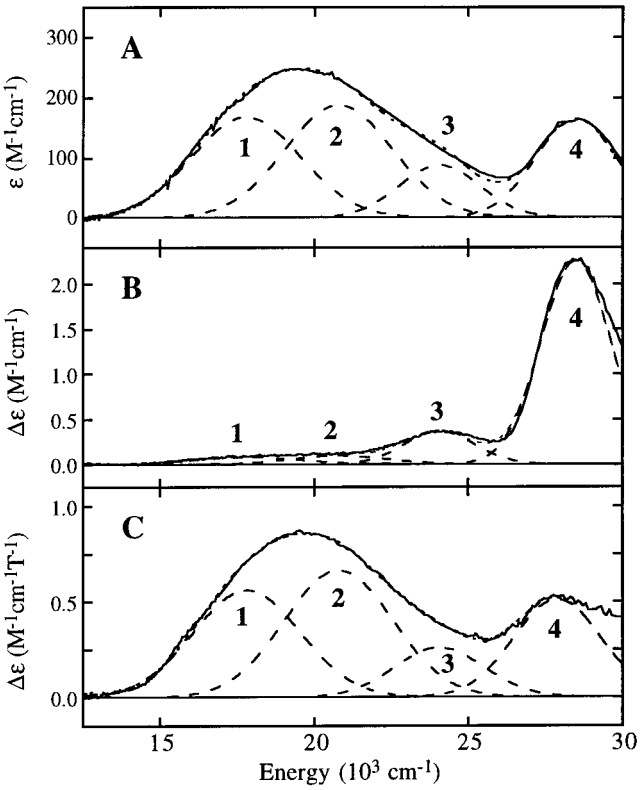

Figure 7. Simultaneous Gaussian fit of the charge-transfer region absorption (A), CD (B), and MCD (C) spectra of CS2+α-KG. The transition energies are summarized in Table 2. Bands 1−3 are assigned as Fe^{2+}-to-α-KG charge-transfer transitions and band 4 as the n → π^* transition in α-KG. The absorption spectrum has been corrected for the intensity due to excess α-KG and the protein tail.

(56) Suzuki, H. *Electronic Absorption Spectra and Geometry of Organic Molecules: An Application of Molecular Orbital Theory*; Academic Press: Inc.: New York, 1967; pp 429−438.

assignment as iron-to-α-KG charge-transfer transitions since similar features are seen for FeAS+α-KG where there is no ligand acceptor orbital other than from α-KG.[53] The n → π^* transition in the CS2+α-KG complex is centered at 27 900 cm^{-1} in the low-temperature MCD and 28 500 cm^{-1} in room-temperature CD/absorption and has shifted to lower energy relative to this transition in apoCS2+α-KG (∼29 000 cm^{-1}). The fact that the n → π^* transition shifts upon metal binding and becomes paramagnetic indicates that the ligand orbitals are directly interacting with the iron. Furthermore, the appearance of the MLCT transitions in the enzyme + cosubstrate complex means that there must be orbital overlap between Fe^{2+} and α-KG, indicating that α-KG binds directly to the metal.

Discussion

Decarboxylation of α-keto acids is hindered by the inability of the carbonyl group to delocalize the negative charge produced. This is overcome by α-keto acid dehydrogenases and decarboxylases by using the coenzyme thiamine pyrophosphate as an electron sink.[57] In the α-KG-dependent non-heme iron enzymes, this is achieved by utilizing O_2 as an electron acceptor for the oxidative decarboxylation process. Despite the large number of α-KG-dependent non-heme enzymes, there is surprisingly little information known about the coordination environment of the ferrous active site. We have sought to address this through the use of CD, MCD, and VTVH MCD spectroscopies to study the multifunctional α-KG-dependent enzyme CS2. CD titrations show that the iron is tightly bound in the active site of the resting enzyme (K_B > 5000 M^{-1}). From the energy ($10Dq$ = 10 050 cm^{-1}) and splitting (Δ^5E_g = 1690 cm^{-1}) of the ligand field transitions, the Fe^{2+} site in resting CS2 is described as six-coordinate distorted octahedral. The ground-state parameters obtained from saturation magnetization analysis ($g_{||}$ = 9.2 and δ = 4.5 cm^{-1}) result in a small splitting of the $^5T_{2g}$ orbital ground state ($\Delta \approx -400$ cm^{-1}, $|V| \approx 190$ cm^{-1}), which supports the six-coordinate assignment. While there is no crystal structure of any α-KG-dependent non-heme iron enzyme, a recent structure of Mn-substituted IPNS, a non-heme enzyme which performs oxidative ring closure similar to CS2, describes the active site as six coordinate with two histidines, one aspartate, one glutamine, and two solvent water ligands.[58] However, although there are several conserved residues between IPNS and other α-KG-dependent enzymes,[3,37] the very low homology to CS2[16] hinders making possible assignments of the iron ligands in CS2 based on the IPNS structure.

The interaction of the α-KG cosubstrate with the CS2 active site has also been investigated. CD titrations show that Fe^{2+} and α-KG are tightly bound in the CS2+α-KG complex (K_B-(Fe^{2+}) > 10 000 M^{-1}, K_B(α-KG) > 5000 M^{-1}) and that α-KG binds better to the iron-containing enzyme than to the apoenzyme. Thus it appears that the presence of Fe^{2+} helps facilitate cosubstrate binding at the active site. The ligand field data for CS2+α-KG show two transitions indicative of a six-coordinate ferrous site ($10Dq$ = 9500 cm^{-1}, Δ^5E_g = 1630 cm^{-1}). However, the six-coordinate Fe^{2+} site in CS2+α-KG is different than that in resting CS2 since the d → d transitions have shifted to lower energy, the sign of the CD spectrum has reversed, and the ground-state spin Hamiltonian parameters are different ($g_{||}$ = 8.7, δ = 2.7 cm^{-1}). The δ value obtained is unusually low for a six-coordinate site and corresponds to a large splitting of the $^5T_{2g}$ state ($\Delta \approx -1000$ cm^{-1}, $|V| \approx 670$ cm^{-1}). This indicates that the Fe^{2+} t_{2g} orbitals, which are sensitive to π-bonding interactions, are significantly perturbed by the presence of α-KG and may be involved in π-back-bonding to the cosubstrate.

The ligand field CD and MCD spectra of CS2+α-KG show indications of additional features to higher energy. It was observed that the addition of α-KG to resting CS2 or the addition of Fe^{2+} to apoCS2+α-KG changes the solutions from colorless to pink, indicating charge-transfer transitions in the visible region. The UV/vis absorption, CD, and MCD spectra of CS2+α-KG show a broad feature at ∼20 000 cm^{-1} (500 nm) which can be resolved into three bands at 17 820, 20 800, and 24 070 cm^{-1}. These low-lying bands, which appear only when Fe^{2+} and α-KG are both present in the active site, are indicative of MLCT transitions and require that there be direct metal−ligand overlap between Fe^{2+} and α-KG. The increased intensity of the charge-transfer transitions for CS2+α-KG relative to FeAS+α-KG reflects an increased Fe^{2+}−α-KG orbital overlap in the enzyme which may be due in part to a more rigid position of the cosubstrate due to electrostatic and hydrophobic interactions of α-KG with the protein.[59] Thus the cosubstrate not only perturbs the ferrous active site in CS2, but in fact binds directly to the metal.

The mode of α-KG binding can be addressed through comparison with ferrous complexes synthesized to model the active site of α-KG-dependent enzymes. To date, three such models have been reported,[60−62] each with Fe^{2+} complexed to the α-keto acid benzoylformate (BF): [Fe^{II}(TPA)(BF)(MeOH)]-(ClO_4)·2MeOH (**1**), [Fe^{II}(6TLA)(BF)](ClO_4) (**2**), and Fe^{II}-(BF)(HB(3,5-Me_2pz)$_3$)(CH_3CN) (**3**).[63] The first of these has a six-coordinate distorted octahedral ferrous site with four ligands derived from the tetradentate TPA ligand, one methanol ligand, and one carboxylate oxygen from BF which is bound monodentate to the iron. **2** and **3** are also six-coordinate, but have the α-keto acid bound bidentate to the iron through one of the carboxylate oxygens and the carbonyl oxygen. The absorption spectrum of **1** shows features at ∼340−420 nm, which are assigned as transitions to the pyridines in the tetradentate ligand, and no lower energy visible transitions.[61] The absorption spectrum of **2**, which is blue-purple in color, shows two additional features at 544 nm (ϵ = 690 M^{-1} cm^{-1}) and 590 nm (sh) in both coordinating and noncoordinating solvents,[60,61] and **3** shows similar absorption features at 555 and 610 nm.[62] These features are attributed to Fe^{2+}-to-α-keto MLCT transitions which occur when the carbonyl oxygen is bound to the iron and which are subsequently absent in the monodentate BF complex, **1**.[61] Comparison of the CS2+α-KG UV/vis spectra indicates that the α-keto−carboxylate moiety of α-KG must be bound bidentate to the metal in the enzyme active site in order to produce the MLCT transitions observed at ∼500 nm. (The higher energy of these transitions in the protein relative to the models is likely due to the substituent on the α-carbon in BF having a larger π conjugation network which stabilizes the π^*

(57) Walsh, C. *Enzymatic Reaction Mechanisms*; W. H. Freeman and Company: San Francisco, 1979; pp 682−697.
(58) Roach, P. L.; Clifton, I. J.; Fülöp, V.; Harlos, K.; Barton, G. J.; Hajdu, J.; Andersson, I.; Schofield, C. J.; Baldwin, J. E. *Nature* **1995**, *375*, 700−704.
(59) Hanauske-Abel, H. M.; Günzler, V. *J. Theor. Biol.* **1982**, *94*, 421−455.
(60) Chiou, Y.-M.; Que, L., Jr. *J. Am. Chem. Soc.* **1992**, *114*, 7567−7568.
(61) Chiou, Y.-M.; Que, L., Jr. *J. Am. Chem. Soc.* **1995**, *117*, 3999−4013.
(62) Ha, E. H.; Ho, R. Y. N.; Kisiel, J. F.; Valentine, J. S. *Inorg. Chem.* **1995**, *34*, 2265−2266.
(63) Abbreviations: TPA, tris(2-pyridylmethyl)amine; 6TLA, tris[(6-methyl-2-pyridyl)methyl]amine; HB(3,5-Me_2pz)$_3$, tris(3,5-dimethyl-1-pyrazolyl)borohydride.

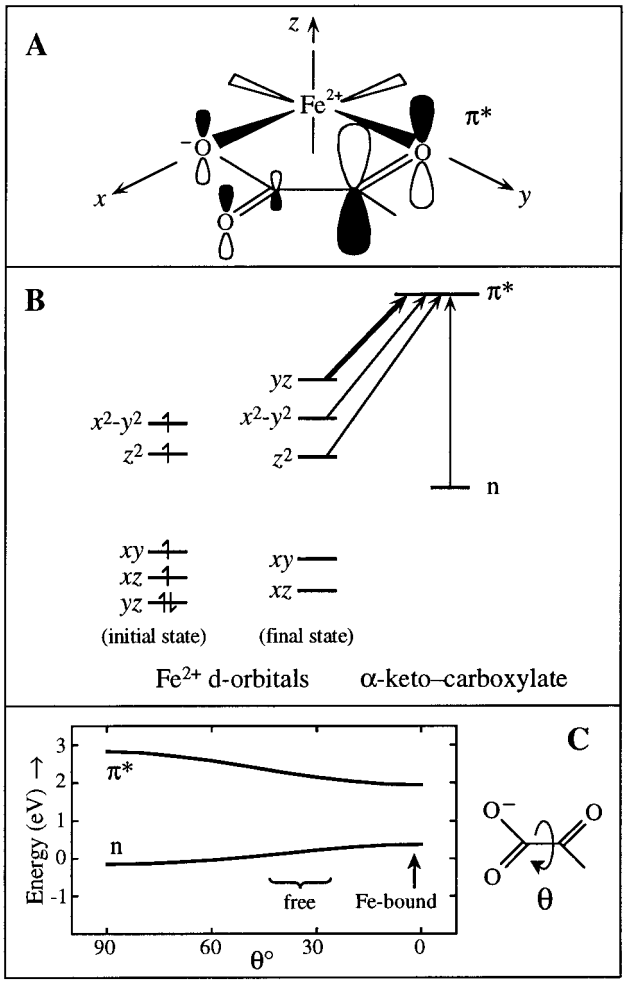

Figure 8. (A) Molecular coordinate scheme describing the Fe^{2+} interaction with the α-keto−carboxylate π^* orbital, where the lobe size reflects the electron density contribution of each atom. (B) MO energy level diagram for CS2+α-KG showing the Fe^{2+} d orbitals prior to (initial state) and upon metal-to-ligand charge transfer (final state) and the pertinent α-keto−carboxylate ligand orbitals. On the basis of overlap and symmetry considerations, predicted transitions are indicated with arrows, the heavier arrow denoting the transition expected to be most intense. (C) Energies of the HOMO (n) and LUMO (π^*) levels as a function of the dihedral angle (θ) between the carbonyl and carboxyl groups of an α-keto−carboxylate moiety. A bracket indicates a representative n/π^* separation for unbound α-KG, which has a twisted conformation, and an arrow indicates this separation when α-KG is locked into a more planar arrangement through binding to iron.

orbital more effectively than does α-KG.) These results show that α-KG binds directly to the iron in a bidentate fashion and must therefore displace two ligands, either endogenous or solvent ligands, from the six-coordinate resting CS2 active site. This provides experimental support for early hypotheses based on prolyl hydroxylase inhibitor studies[59,64] which propose that α-KG binds bidentate to the metal through the α-keto acid moiety.

A more rigorous assignment of the charge-transfer transitions observed for CS2+α-KG is made through consideration of the Fe^{2+} and α-KG molecular orbital (MO) interactions. Density functional calculations have been performed on pyruvate as a simple α-keto acid to obtain MO descriptions for the α-keto−carboxylate moiety in α-KG. These calculations, as well as those performed on the dianionic form of α-KG, show a single π^* LUMO orbital available for charge transfer and no other acceptor orbitals within 2 eV. Figure 8A describes the interaction of this π^* orbital with the iron active site in CS2+α-KG and shows that the π^* is primarily composed of p_z density on the carbonyl, with some conjugation to the carboxylate p_z orbitals. Thus the Fe^{2+} d_{yz} orbital, which is pointing directly toward the carbonyl in the coordinate frame of Figure 8A, should have the most overlap with the π^* orbital and, therefore, be the most stabilized. This is shown in Figure 8B, which qualitatively describes the five iron d orbitals prior to (initial state) and upon metal-to-ligand charge transfer (final state), including the loss of electron repulsion in the d_{yz} ground-state orbital. From overlap considerations, a single MLCT transition is predicted from the Fe^{2+} d_{yz} orbital to the α-keto−carboxylate π^* orbital, as indicated by the heavy arrow in Figure 8B. Experimentally, however, three MLCT transitions are observed. Because there is only one π^* orbital available for charge transfer and there are three MLCT transitions within ∼6000 cm^{-1} of each other, the two additional transitions likely originate from the Fe^{2+} $d_{x^2-y^2}$ and d_{z^2} orbitals, as depicted in Figure 8B, which gain intensity through configurational interaction.

Additional information about cosubstrate binding can be obtained through monitoring the higher-energy α-KG n → π^* transition, which is observed at ∼31 500 cm^{-1} in the absorption spectrum of aqueous α-KG. When α-KG is added to apoCS2, the n → π^* transition shifts to lower energy (∼29 000 cm^{-1} in CD) which may be attributed to the large change in the dielectric constant from ∼80 in an aqueous environment to ∼5 in the protein. The fact that this transition becomes CD-active when α-KG is bound to apoCS2 indicates that the cosubstrate has a chiral arrangement within the enzyme. When α-KG binds to resting CS2 (i.e., with iron present) the n → π^* transition shifts to even lower energy than when bound to apoCS2 (from ∼29 000 cm^{-1} to ∼27 900 cm^{-1}). Control studies find that the n → π^* transition in FeAS+α-KG is similarly shifted to lower energy relative to in aqueous α-KG (from ∼31 500 cm^{-1} to ∼30 500 cm^{-1}). Calculations show that the α-keto−carboxylate HOMO orbital ("n") is composed of p_x and p_y density primarily localized on the carboxylate, with some conjugation to the p_x and p_y orbitals of the α-carbonyl. When α-KG binds to iron, one expects that the metal−ligand interaction would stabilize the ligand n orbital, which is primarily localized on the carboxylate, and destabilize the π^* orbital, primarily localized on the carbonyl, thereby increasing the n → π^* transition energy. However, the opposite is observed experimentally for both CS2+α-KG and FeAS+α-KG. This can be explained in terms of the conjugation within the α-keto acid moiety of α-KG. Density function calculations on pyruvate show that the n/π^* separation changes as a function of the dihedral angle between the carbonyl and carboxyl groups (θ) and reaches a minimum when the two are coplanar and have maximum conjugation (Figure 8C), analogous to what is found for conjugated α,β-dicarbonyl compounds.[56] Unbound α-KG is expected to have a twisted arrangement, so the fact that the n → π^* transition energy decreases when α-KG binds to iron suggests that the α-keto carboxylate moiety becomes significantly more planar, as indicated in Figure 8C.

On the basis of these results, we can now draw the first two steps in the mechanism for CS2 as shown in Scheme 3: Fe^{2+} binds to the active site to form a six-coordinate distorted octahedral site, followed by addition of α-KG which binds in a bidentate fashion to the metal with the α-keto-carboxylate moiety nearly planar, forming a five-membered ring with the iron. The next step in several proposed mechanisms involves

(64) Majamaa, K.; Hanauske-Abel, H. M.; Günzler, V.; Kivirikko, K. I. *Eur. J. Biochem.* **1984**, *138*, 239−245.

Scheme 3

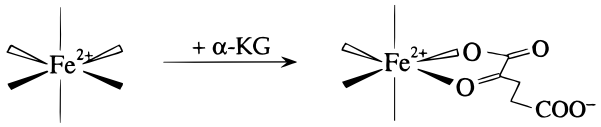

the binding of O_2 to the iron to create a ferric−superoxide species which then attacks the α-carbon of α-KG, followed by release of CO_2.[1,2] If dioxygen binds to CS2+α-KG by displacing a ligand axial to the five-membered ring, then having α-KG bound bidentate to the iron would properly position the cosubstrate at the active site for nucleophilic attack by superoxide. Considering the reactivity of the three α-keto acid model compounds with O_2, all of which result in quantitative decarboxylation of BF to benzoic acid and CO_2,[60−62] decarboxylation appears to be more effective when the α-keto−carboxylate moiety can retain the bidentate binding mode to the iron. Models **1** and **2** have four ligands fixed by their tetradentate ligand groups and would require the α-keto acid to become monodentate in order for O_2 to bind to the iron. Decarboxylation of BF by these models occurs at a significantly slower rate than that of model **3** (days vs minutes), which has a tridentate ligand group and an exchangeable solvent ligand and could thereby retain the bidentate binding mode of BF.[62]

The presence of the MLCT transitions for CS2+α-KG indicates some degree of π-back-bonding between Fe^{2+} and α-KG, as supported by the large splitting of the d_π orbitals. This back-bonding may serve a mechanistic purpose, perhaps by activating the α-KG for reaction with oxygen through imparting some radical character to the cosubstrate or by activating the iron center for reaction with dioxygen. Significant π-back-bonding has been also observed in the non-heme iron anticancer agent bleomycin,[65,66] in which the back-bonding serves to stabilize the initial $Fe^{3+}-O_2^-$ intermediate from loss of superoxide and promotes the formation of the ferric−peroxy activated bleomycin species.[44,67] It should be noted, however, that the MLCT transitions observed for CS2+α-KG are less intense than those observed for bleomycin, indicating a weaker covalent interaction. Thus, the back-bonding in CS2+α-KG may not be as significant and may simply reflect the fact that α-KG is coordinated in a bidentate fashion at the active site.

It is interesting to compare the cosubstrate interactions in CS2 with those of the non-heme iron enzyme phenylalanine hydroxylase (PAH), which also requires an organic cosubstrate for catalysis, tetrahydrobiopterin (BH_4).[68,69] As with CS2, an uncoupled reaction is known to occur for PAH in which BH_4 is oxidized without the hydroxylation of substrate. The rate of the uncoupled reaction in PAH is similar to that of the substrate coupled reaction,[69] while in CS2, the uncoupled reaction occurs at a significantly slower rate. Also in contrast to CS2, the addition of cosubstrate to PAH causes no change to the resting ferrous site,[70] whereas the cosubstrate binds directly to the metal in CS2. These differences may be due to differences in reactivity between the two cofactors: while α-KG by itself is unreactive with O_2, tetrahydrobiopterins are known to autooxidize fairly quickly in aerobic neutral solutions. Thus CS2 may require α-KG to bind to the iron in order to activate the cosubstrate for reaction.

In summary, these studies provide the first spectroscopic probe of the ferrous active site in CS2, a particularly interesting enzyme which catalyzes oxidative ring closure and desaturation chemistry, as well as α-KG-dependent hydroxylation, depending on the substrate. The resting enzyme is described as six-coordinate distorted octahedral and has fairly typical ligand field splittings for O and N ligation. Addition of the α-KG cosubstrate perturbs the Fe^{2+} coordination environment and increases the ground-state ligand field splittings, indicating π-back-bonding with the metal. Upon α-KG binding, new low-energy MLCT transitions are observed which requires direct metal−ligand overlap. Comparison with models shows that α-KG binds in a bidentate fashion, thereby displacing two ligands from the resting active site. Furthermore, changes in the α-KG n → π^* transition, which becomes CD and MCD active upon cosubstrate binding, support a nearly planar arrangement of the α-keto−carboxylate moiety. As decarboxylation of α-KG to generate succinate, CO_2, and a reactive high-valent iron−oxygen species is purported to occur before hydroxylation, cyclization, or desaturation, the spectroscopic characterization of the active site with α-KG bound provides insight into the catalytic mechanism. These results suggest that binding of α-KG may be necessary either to activate the inert cosubstrate for reaction with dioxygen directly, through imparting some radical character to α-KG via π-back-bonding, or to position the α-keto group of the cosubstrate for attack by an iron−oxygen species formed through O_2 activation by the iron center.

Acknowledgment. This research was supported by grants from the National Institutes of Health (GM40392, E.I.S., and AI14937, C.A.T.). The computing facilities of the Stanford Department of Chemistry are supported, in part, by a grant from the National Science Foundation (CHE-9408185).

JA972408A

(65) Stubbe, J.; Kozarich, J. W. *Chem. Rev. (Washington, D.C.)* **1987**, *87*, 1107−1136.
(66) Petering, D. H.; Byrnes, R. W.; Antholine, W. E. *Chem.-Biol. Interact.* **1990**, *73*, 133−182.
(67) Westre, T. E.; Loeb, K. E.; Zaleski, J. M.; Hedman, B.; Hodgson, K. O.; Solomon, E. I. *J. Am. Chem. Soc.* **1995**, *117*, 1309−1313.
(68) Shiman, R. In *Folates and Pterins: Chemistry and Biochemistry of Pterins*; Blakely, R. L., Benkovic, S. J., Eds.; John Wiley & Sons: New York, 1985; Vol. 2, pp 179−249.
(69) Kappock, T. J.; Caradonna, J. P. *Chem. Rev. (Washington, D.C.)* **1996**, *96*, 2659−2756.
(70) Kemsley, J. N.; Loeb, K. E.; Mitić, N.; Caradonna, J. P.; Solomon, E. I., manuscript in preparation.